

# Trajectory Tracking Control of Tilt-Wing eVTOL Using Aerodynamic Coupling Observer and Wing Angle Correction Method

Takuma Katagiri, Kota Fujimoto, Sakahisa Nagai and Hiroshi Fujimoto  
*The University of Tokyo, Kashiwa, Japan*  
 Correspondence author's email: katagiri.takuma23@ae.k.u-tokyo.ac.jp

**Abstract**—Recently, electric vertical take-off and landing has been attracting attention as a potential solution for alleviation of urban traffic congestion, alternative tools of delivery, and inspection missions in disaster situations. We focus on the advantages of the tilt-wing type, such as the low drag of the wing during ascent and the ability to use the propeller wake even during transition phase to control the lift by flap. This paper focuses on the how to determine the tilt angle reference to track the desired trajectory. Some previous research uses the tilt angle that achieve trim state as the reference. It has a disadvantage that the actuator in the inner layer saturates when the high acceleration command is given or when wind disturbance exists. Proposed wing angle correction method enables aircraft to track the trajectory even in those situations by correcting the tilt angle to solve a optimization problem that considers the actuator input and disturbance estimated by the inner layer DOB. The results of the numerical simulation and hardware in the loop simulation show that the proposed control system reduces the actuator saturation and improves the trajectory tracking performance.

**Index Terms**—trajectory tracking, unmanned aerial vehicle, eVTOL, tilt-wing.

## I. INTRODUCTION

### A. Research trends in eVTOL

Recently, electric vertical take-off and landing (eVTOL) has been expected to play a role in various scenarios such as transportation, last-mile delivery, and inspection in the event of a disaster [1], [2]. It is owing to technological development such as high-performance batteries, electric propulsion technology, and autonomous driving technology [3]–[5]. Electric propulsion technology is especially important for an eVTOL system. Electric propulsion has the advantages of quick thrust control with high torque response [6], accurate torque estimation, and power regeneration [7]. It leads developing new control methods such as wind speed estimation using motor current [8] and fast and efficient thrust control of variable pitch propellers [9].

There are a lot of configurations in eVTOL, and a tilt-wing type as shown in Fig. 1(a) is one of the promising configurations. It has the advantages of high energy efficiency in cruise mode and low drag of the wing during ascent. In addition, the propeller wake can be used to control the lift by flap even in low-velocity flight. In this paper, we focus on the tilt-wing type eVTOL.

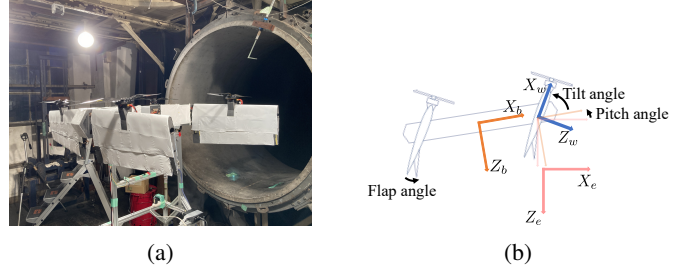


Fig. 1: (a) Quad tilt-wing aircraft. (b) Schematic figure of the aircraft.  $[X_e, Z_e]$  is the earth-fixed coordinate system,  $[X_b, Z_b]$  is the body coordinate system and  $[X_w, Z_w]$  is the wing coordinate system.

### B. Research trends in tilt-wing eVTOL

A tilt-wing eVTOL often faces instability during the transition phase due to the changes of aerodynamic characteristics when the wing angle changed. To mitigate this problem, a lot of studies have focused on attitude control and velocity control of the tilt-wing eVTOL. [10]–[13].

In [10], a flight control system was developed for a tandem tilt-wing aircraft, and the stability of the longitudinal and lateral motion was discussed. In addition, the complete transition from hover mode to cruise mode was performed under the control of the pilot; however, velocity control is not considered. In [11], the velocity control of a tilt-wing aircraft was achieved using a feedforward controller derived from wind tunnel experiments. However, the flight test results showed a steady-state error in the velocity response. In [12], flight tests were conducted to verify the velocity control in the transition state. The flight test showed good performance to track the velocity command in the vertical and horizontal directions. However, there are three points that have not been discussed. The first point is the robustness against wind disturbances. The second is the performance degradation caused by modeling errors resulting from linearization. The last is that the actuator may saturate when the high acceleration command is given or wind disturbance exists. In [13], which is written by the same group of [12], a nonlinear model predictive control (NMPC) was employed for velocity control. It shows a good velocity control performance for the vertical and horizontal directions. However, due to the high computational cost, the NMPC

sampling time is 0.1s, which is slow considering the motor response. To enhance the disturbance rejection performance, the inner layer controller needs to be sophisticated.

### C. Contribution of this paper

The main features of our proposed controller are as follows:

- The inner layer controller that achieves fast suppression of the disturbance and the modeling error by the propellers and flaps.
- The outer layer controller that corrects the wing angle so that the actuator in the inner layer does not saturate.

In [14], the velocity controller which employs disturbance observer (DOB) as the inner layer controller was proposed. DOB is widely applied in various fields such as electric vehicles, robotics, and drones because of its effectiveness and simplicity [15], [16], and it has proven to be also effective in the velocity control of tilt-wing eVTOL.

In this paper, we propose a new outer layer controller that corrects the wing angle so that the actuator in the inner layer does not saturate. The tilt angle is usually determined by the outer layer controller because the tilt actuator cannot move as quick as the propeller actuator and the flap actuator due to the large moment of inertia of the wing. Some research used the tilt angle that achieve trim state as the tilt angle reference [11], [12]. However, it has a disadvantage that the actuator in the inner layer saturates when the high acceleration command is given. The saturation of the actuator is undesirable because it reduces the room for reacting to the wind disturbance or aerodynamic modeling errors. On the contrary, our proposed method reduces the actuator saturation and improves the trajectory tracking performance even the dynamic trajectory or the situation where wind disturbance exists. It is achieved by determining the tilt angle by solving a optimization problem that considers the acceleration command and disturbance estimated by the inner layer DOB. The proposed method is validated in the numerical simulation and the hardware in the loop simulation (HILS).

## II. PROPOSED CONTROL SYSTEM

The schematic figure of the aircraft is shown in Fig. 1(b). This paper focuses on the aircraft motion in  $[X_e, Z_e]$  plane. Overview of the control system is shown in Fig. 2. The parameter definitions are listed in Table I.

The position controller produces the acceleration commands to track the desired trajectory. The acceleration of the aircraft is controlled by the tilt angle correction block and acceleration controller block. The tilt angle correction block is the outer layer that corrects the wing angle so that the actuator in the inner layer do not saturates. The inner layer controller is the acceleration controller that produces the propeller rotational speed commands and flap angle commands. The attitude controller controls the pitch angle of the aircraft by the difference of the front and rear propeller thrust and the flap lift. The mixing block blends the output of the attitude controller and the acceleration controller. Each control block is detailed in the following subsections.

TABLE I: Parameter definitions.

Parameter	Definition	Unit
$m$	mass of aircraft	kg
$I_{yy}$	inertia of aircraft around $Y_b$ axis	kg m <sup>2</sup>
$\omega$	propeller angular velocity	rad/s
$\delta$	flap angle	deg
$\sigma$	tilt angle	deg
$\theta_{\text{fuselage}}$	pitch angle of aircraft body	rad
$\theta_{\text{wing}}$	angle between main wing and ground	rad
$\mathbf{r} = [X, Z]^T$	position of aircraft	m
$\mathbf{V} = [V_x, V_z]^T$	velocity of aircraft	m/s
$\mathbf{a} = [a_x, a_z]^T$	acceleration of aircraft	m/s <sup>2</sup>
$\mathbf{v}$	airspeed vector	m/s
$\mathbf{F}_{\text{th}}$	force vector produced by the propeller thrust	N
$\mathbf{F}_{\text{aero}}$	aerodynamic force vector	N
$\mathbf{F}_{\text{g}}$	gravity vector	N
$M_{\text{th}}$	moment produced by the propeller thrust	N m
$M_{\text{aero}}$	moment produced by the wing	N m
$(\cdot)_e$	variables in the earth fixed coordinates	-
$(\cdot)_w$	variables in the wing coordinates	-
$(\cdot)_b$	variables in the body coordinates	-
$(\cdot)$	limited variables	-
$(\cdot)^*$	reference value	-
$(\cdot)_0$	operating point	-
$(\cdot)_{\text{cent}}$	center of the achievable range of the actuator	-
$\Delta(\cdot)$	deviation from the operating point	-
$(\cdot)_{\text{tot}}$	output of the acceleration controller	-
$(\cdot)_{\text{fr}}$	output of the attitude controller	-
$(\cdot)_f$	value of the front actuator	-
$(\cdot)_r$	value of the rear actuator	-
$(\cdot)^+$	psuedo-inverse matrix of $(\cdot)$	-

### A. Mixing

The mixing block blends the output of the attitude controller and the acceleration controller as

$$\begin{bmatrix} \omega_f^* \\ \omega_r^* \\ \delta_f^* \\ \delta_r^* \end{bmatrix} = \begin{bmatrix} \omega_0 + \Delta\tilde{\omega}_{\text{tot}}^* + \Delta\tilde{\omega}_{\text{fr}}^* \\ \omega_0 + \Delta\tilde{\omega}_{\text{tot}}^* - \Delta\tilde{\omega}_{\text{fr}}^* \\ \delta_0 + \Delta\tilde{\delta}_{\text{tot}}^* + \Delta\tilde{\delta}_{\text{fr}}^* \\ \delta_0 + \Delta\tilde{\delta}_{\text{tot}}^* - \Delta\tilde{\delta}_{\text{fr}}^* \end{bmatrix}. \quad (1)$$

Operating point  $[\omega_0, \delta_0]^T$  is the actuator value that balances the forces acting on the aircraft at each airspeed  $v_{x_b}$  and wing angle  $\theta_{\text{wing}}$ .

### B. Limit of the actuator output

We consider the saturation of the actuator output. To prevent the wind up of each controller, the output of the attitude controller and the acceleration controller is limited in each controller as shown in Figs. 3 and 4. Though the attitude control is essential for the safety flight, we consider the limit of the attitude controller output firstly. To ignore the operating points  $[\omega_0, \delta_0]^T$  and output of the acceleration controller  $[\Delta\omega_{\text{tot}}, \Delta\delta_{\text{tot}}]^T$  in (1), the limit of the attitude controller is given as follows:

$$-\Delta\omega_{\text{fr},\text{max}} \leq \Delta\tilde{\omega}_{\text{fr}}^* \leq \Delta\omega_{\text{fr},\text{max}}, \quad (2)$$

$$-\Delta\delta_{\text{fr},\text{max}} \leq \Delta\tilde{\delta}_{\text{fr}}^* \leq \Delta\delta_{\text{fr},\text{max}}. \quad (3)$$

$\Delta\omega_{\text{fr},\text{max}}$  and  $\Delta\delta_{\text{fr},\text{max}}$  are given as follows:

$$\Delta\omega_{\text{fr},\text{max}} = \frac{\omega_{\text{max}} - \omega_{\text{min}}}{2}, \quad (4)$$

$$\Delta\delta_{\text{fr},\text{max}} = \frac{\delta_{\text{max}} - \delta_{\text{min}}}{2}, \quad (5)$$

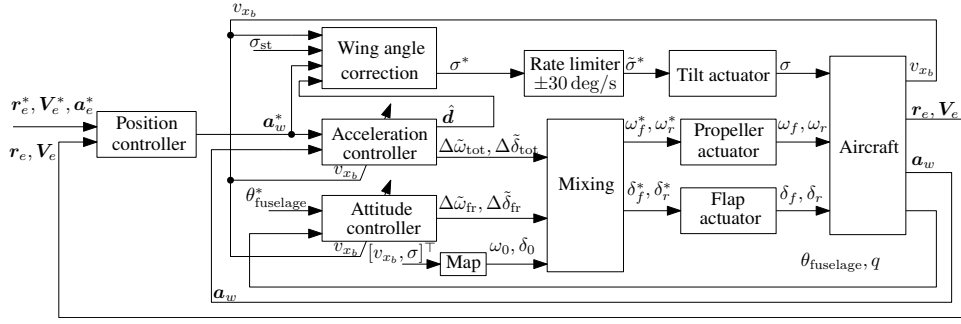


Fig. 2: Overview of the proposed control system.

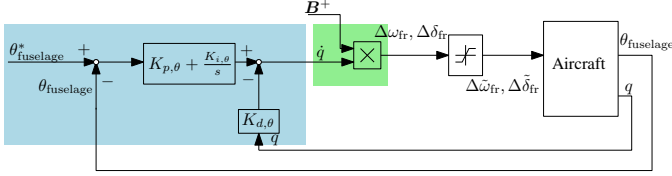


Fig. 3: Attitude controller (The blue part is the PI-D controller and the green part is the control allocation).

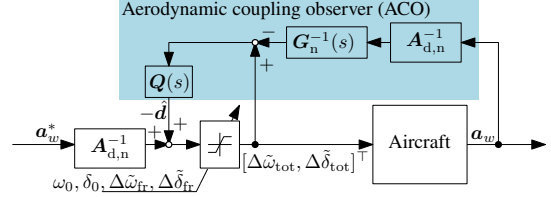


Fig. 4: Acceleration controller.

where  $\omega_{\max}$  and  $\omega_{\min}$  are the maximum and minimum propeller speed, respectively.  $\delta_{\max}$  and  $\delta_{\min}$  are the maximum and minimum flap angle, respectively.

Next, we consider the limit of the acceleration controller output. Taking into account the output of the attitude controller and the operating points based on (1), the limit of the acceleration controller is given as follows:

$$\omega_{\min} - \omega_0 + |\Delta\tilde{\omega}_{\text{fr}}^*| \leq \Delta\tilde{\omega}_{\text{tot}}^* \leq \omega_{\max} - \omega_0 - |\Delta\tilde{\omega}_{\text{fr}}^*|, \quad (6)$$

$$\delta_{\min} - \delta_0 + |\Delta\tilde{\delta}_{\text{fr}}^*| \leq \Delta\tilde{\delta}_{\text{tot}}^* \leq \delta_{\max} - \delta_0 - |\Delta\tilde{\delta}_{\text{fr}}^*|. \quad (7)$$

### C. Attitude control

The attitude control is performed by a PI-D controller and control allocation. The structure is shown in Fig. 3. The blue part is the PI-D controller and it generates the desired pitch angular acceleration. The gain of the controller is designed by the pole placement for the nominal plant  $\frac{1}{s^2}$ . The pitching moment is generated by the difference in the front and rear propeller thrusts and the flap lift. It indicates that the aircraft has redundant actuators for attitude controller, therefore the control allocation to the propellers and flaps is needed. The control allocation is performed by multiplying the pseudo-inverse matrix of the matrix  $\mathbf{B}$  and it is expressed as follows:

$$\dot{q} = \mathbf{B} \begin{bmatrix} \Delta\omega_{\text{fr}} \\ \Delta\delta_{\text{fr}} \end{bmatrix}. \quad (8)$$

The size of the matrix  $\mathbf{B}$  is  $1 \times 2$ , and scheduled by the airspeed. The matrix  $\mathbf{B}$  is obtained from the wind tunnel test. The output of the control allocation is limited by the saturation block detailed in (2) and (3).

### D. Acceleration control

The acceleration control is achieved by the aerodynamic coupling observer (ACO). This is the name given to the DOB

based on the acceleration measurement in wing coordinates proposed in [14]. By using the ACO, the acceleration parallel to the wing is controlled by the propellers and the acceleration perpendicular to the wing is controlled by the flaps independently. The structure is shown in Fig. 4. In the figure,  $\mathbf{A}_{\text{d},\text{n}}$  is a diagonal part of a nominal matrix of  $\mathbf{A}$  which is expressed as follows:

$$\begin{bmatrix} a_{x_w} \\ a_{z_w} \end{bmatrix} = \mathbf{A} \begin{bmatrix} \Delta\omega_{\text{tot}} \\ \Delta\delta_{\text{tot}} \end{bmatrix}. \quad (9)$$

The matrix  $\mathbf{A}_{\text{d},\text{n}}$  is scheduled by the airspeed, and it is obtained from the wind tunnel test.  $\mathbf{G}_{\text{n}}(s)$  is a nominal actuator dynamics matrix, and it is expressed as follows:

$$\mathbf{G}_{\text{n}}(s) = \text{diag} \left\{ \frac{1}{\tau_{\text{th},\text{n}}s + 1}, \frac{1}{\tau_{\delta,\text{n}}s + 1} \right\}, \quad (10)$$

where  $\tau_{\text{th},\text{n}}$  and  $\tau_{\delta,\text{n}}$  are the nominal time constant of the propeller and flap actuator dynamics, respectively.  $\mathbf{Q}(s)$  is a low-pass filter and it is expressed as follows:

$$\mathbf{Q}(s) = \text{diag} \left\{ \frac{\omega_{\text{DOB}}}{s + \omega_{\text{DOB}}}, \frac{\omega_{\text{DOB}}}{s + \omega_{\text{DOB}}} \right\}, \quad (11)$$

where  $\omega_{\text{DOB}}$  is the cut-off frequency of the disturbance observer, and it is determined by trial and error. The ACO estimates the disturbance  $\mathbf{d}$  as the dimension of the actuator reference and suppresses it. For the output of the acceleration controller, the variable limiter is used to prevent the wind up explained in (6) and (7).

### E. Position control

The position controller generates the acceleration command in wing coordinates. It consists of the major position control loop, the minor velocity control loop, and feedforward command of the velocity and acceleration reference. The structure

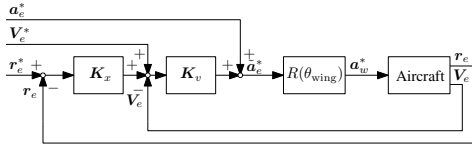


Fig. 5: Position controller.

is shown in Fig. 5.  $K_x$  and  $K_v$  are designed by the pole placement for the nominal plant  $\frac{1}{s^2}$ .  $R(\theta)$  is the rotation matrix which is defined as follows:

$$R(\theta) = \begin{bmatrix} \cos \theta & -\sin \theta \\ \sin \theta & \cos \theta \end{bmatrix}. \quad (12)$$

$\theta_{\text{wing}}$  is the angle between wing and ground. Multiplying  $R(\theta_{\text{wing}})$  indicates the rotation from the earth fixed coordinate system to the wing coordinate system.

#### F. Wing angle correction method

In some previous research, the tilt angle reference is given by the trim of the aircraft [11], [12]. This method is effective in low-acceleration situations. However, in high-acceleration situations, the actuator used in the acceleration controller may saturate and the desired acceleration may not be achieved. To prevent this, it is necessary to consider the saturation of each actuator and change the wing angle so that the actuator does not saturate. In this paper, we propose a method to approximate the achievable acceleration as a rectangle field with sides parallel to the wing, and determine the rectangle by using the relationship in (9), the estimated disturbance  $\hat{d}$ , and the operating point  $[\omega_0, \delta_0]^T$ . Then, the wing angle command is given every 0.1s so that the acceleration command is as close as possible to the center of the achievable acceleration. This method performs transition with less saturation of the actuator, and maximizes the room for reacting to the wind disturbance or aerodynamic modeling errors.

Using the relationship of the acceleration of the aircraft and the output of the acceleration controller in (9), the proposed method comes down to solving the following optimization problem:

$$\min_{\sigma^*} \|W_1 S_1 (A_{d,n}^{-1} R(\sigma^*) a_e^* - \hat{d} + u_0(\sigma^*) - u_{\text{cent}})\|_{\infty} + W_2 S_2 |\sigma_{\text{st}} - \sigma^*| + W_3 S_3 |\sigma_{\text{prev}} - \sigma^*| \quad (13)$$

$$\text{s.t. } \sigma^* \in [5, 90], \quad (14)$$

where  $\hat{d} = [\hat{d}_{\text{th}}, \hat{d}_{\delta}]^T$ ,  $u_0 = [\omega_0, \delta_0]^T$ ,  $u_{\text{cent}} = [\omega_{\text{cent}}, \delta_{\text{cent}}]^T$ . Though the range of the flap angle is not symmetric about 0 deg,  $\delta_{\text{cent}}$  is set at 0 deg.  $S_1$  and  $S_2$  are scaling factors to normalize the each term by the range of each actuators,  $W_1$ ,  $W_2$  and  $W_3$  are weighting coefficients which are determined by the trial and error. The first term is the infinite norm of the difference between the acceleration command transformed into the actuator command and the center of the actuator output range. It evaluates how close the actuator commands are to the saturation at each tilt angle. The second term is the penalty for the trim wing angle, and the third term is the penalty for the previous solution to prevent violent changes in the solution. This optimization problem is solved using a brute-force search

TABLE II: Aircraft parameter.

Symbol	Description	Value
$m$	mass of aircraft	7.7 kg
$-$	wingspan	1.4 m
$S_a$	wing area	0.73 m <sup>2</sup>
$S_s$	wing area in slipstream	0.58 m <sup>2</sup>
$D_p$	propeller diameter	0.58 m
$l_x$	distance between CoG and main wing	0.40 m
$I_{yy}$	moment of inertia of aircraft around Y axis	0.8 kg m <sup>2</sup>

TABLE III: Controller settings in the simulation.

Symbol	Description	Value
$-$	Pole of position controller	-0.75 rad/s
$-$	Pole of attitude controller	-2 rad/s
$\omega_{\text{DOB}}$	Cutoff frequency of the DOB	5 rad/s
$W_1$	Weighting coefficient 1	diag {0.5, 1}
$W_2$	Weighting coefficient 2	0.3
$W_3$	Weighting coefficient 3	0.1

with 5-degree intervals. This solution is applied because the evaluation function is not unimodal.

### III. SIMULATION

The simulation is conducted based on the control system shown in Fig. 2. We conducted two simulations. The tracking performance in dynamic trajectory is evaluated in the first simulation, and the robustness against the wind disturbance is evaluated in the second simulation. The aircraft parameters are shown in Table II, and the simulation parameters are shown in Table III. The simulation model is built based on [14], and modified for quad tilt-wing type and including pitch dynamics.

In the first simulation, the assumed situation is that the aircraft moves from hovering state to the forward flight state while tilting its wings at first, and back to the hovering state finally. Simulation results of the first situation are shown in Fig. 6. Conv. means the conventional method that the tilt angle command is given by the trim of the aircraft according to velocity command. Prop. means the proposed method that the tilt angle command is given by the wing angle correction method. Figs. 6(a) and 6(b) show that the proposed method has less tracking error because the tilt angle is corrected to prevent the actuator saturation as shown in Fig. 6(c). Fig. 6(e) indicates that the proposed method reduced the duration of the saturation. Hence the proposed method has better tracking performance than the conventional method.

In the second simulation, the wind disturbance is added when the aircraft trajectory is set at a constant ground speed. The simulation results are shown in Fig. 7. The headwind is increased by a wind disturbance as shown in Fig. 7(a). The conventional method has large tracking error as shown in Figs. 7(b) and 7(c) because the flap actuator saturates as shown in Fig. 7(f). This is because the tilt angle is not changed even when the achievable acceleration changes by the wind disturbance as shown in Fig. 7(d). On the other hand, the proposed method has good tracking performance than the

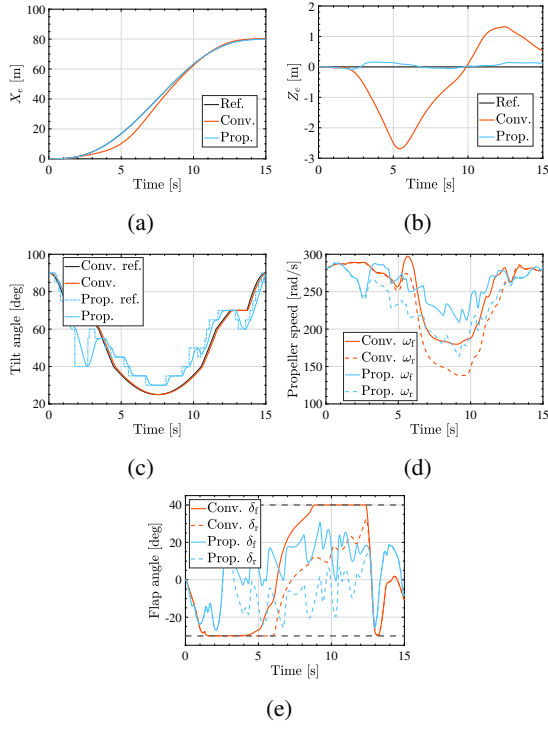


Fig. 6: Simulation results for evaluating tracking performance for dynamic trajectory. (a) Position in  $X$  direction. (b) Position in  $Z$  direction. (c) Tilt angle (reference is before limited by rate limiter). (d) Propeller speed. (e) Flap angle.

conventional method because the tilt angle changed properly considering the achievable acceleration field.

#### IV. EXPERIMENT

The HILS is conducted in the same situation as the second simulation to validate the proposed method. The first situation is not conducted because wind tunnel cannot generate the dynamic and precise wind which is the same as the actual trajectory. The experimental setups are shown in Fig. 8. The force and moment acting on the aircraft are measured by the 6-axis load cell under the body. Only the wind sensor 2, which is placed on the nose of the aircraft, is logged.

The block diagram of the HILS is shown in Fig. 9. The simulator block calculates the aircraft dynamics to satisfy following equations:

$$m \left( \frac{d}{dt} \begin{bmatrix} V_{x,b,\text{sim}} \\ V_{z,b,\text{sim}} \end{bmatrix} + \begin{bmatrix} qV_{z,b,\text{sim}} \\ -qV_{x,b,\text{sim}} \end{bmatrix} \right) = \mathbf{F}_{\text{th}} + \mathbf{F}_{\text{aero}} + \mathbf{F}_{\text{g}}, \quad (15)$$

$$\frac{d}{dt} \mathbf{r}_{e,\text{sim}} = \mathbf{V}_{e,\text{sim}} \quad (16)$$

$$I_{yy} \frac{d}{dt} q_{\text{sim}} = M_{\text{th}} + M_{\text{aero}}, \quad (17)$$

$$\frac{d}{dt} \theta_{\text{sim}} = q_{\text{sim}}. \quad (18)$$

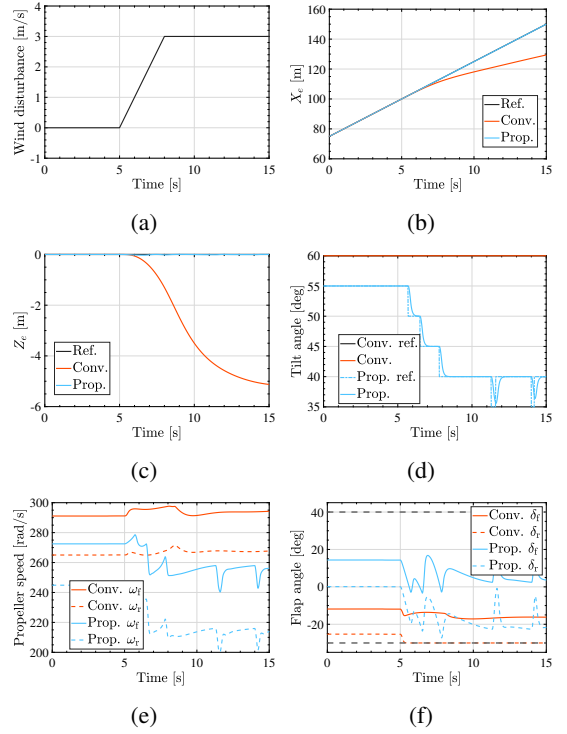


Fig. 7: Simulation results for evaluating robustness to the wind disturbance. (a) Wind disturbance. (b) Position in  $X$  direction. (c) Position in  $Z$  direction. (d) Tilt angle (reference is before limited by rate limiter). (e) Propeller speed. (f) Flap angle.

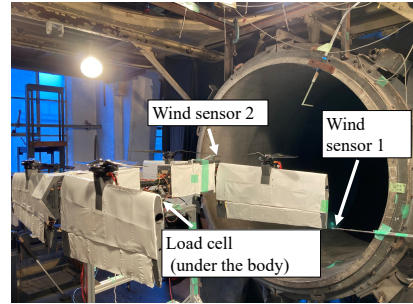


Fig. 8: Experimental setups.

$\mathbf{F}_{\text{th}} + \mathbf{F}_{\text{aero}}$  and  $M_{\text{th}} + M_{\text{aero}}$  is a measured value by the 6-axis load cell.  $\mathbf{F}_{\text{g}}$  is the gravity that added to the load cell measurement.

The controller settings are shown in Table IV. The aircraft mass is set to 5.0 kg.

The HILS result is shown in Fig. 10. The wind speed is

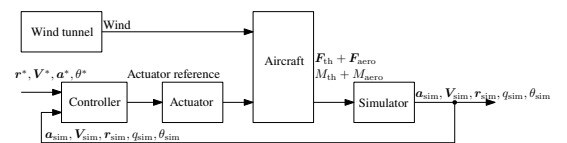


Fig. 9: Block diagram of HILS.

TABLE IV: Controller settings in the HILS.

Symbol	Description	Value
—	Pole of position controller	$-0.35 \text{ rad/s}$
—	Pole of attitude controller	$-2, -1 \pm j\sqrt{3} \text{ rad/s}$
$\omega_{\text{DOB}}$	Cutoff frequency of the DOB	$1.5 \text{ rad/s}$
$W_1$	Weighting coefficient 1	$\text{diag}\{0.5, 1\}$
$W_2$	Weighting coefficient 2	0.4
$W_3$	Weighting coefficient 3	0.2

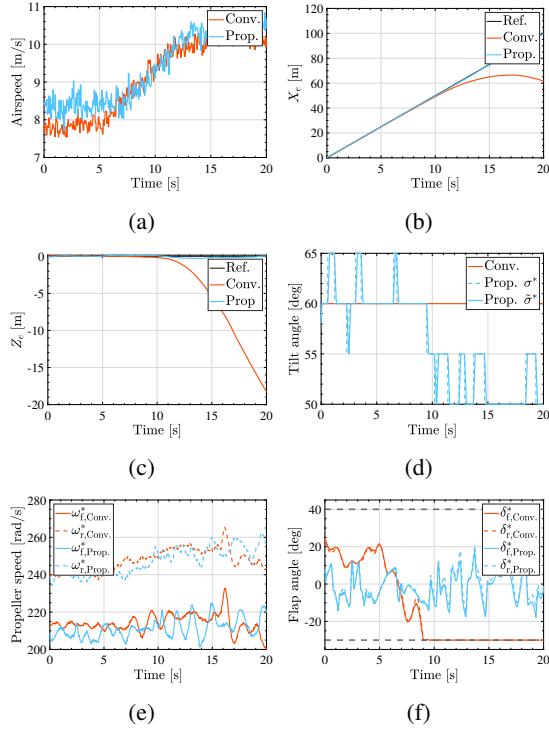


Fig. 10: HILS result. (a) Airspeed. (b) Position in  $X$  direction (c) Position in  $Z$  direction. (d) Tilt angle reference. (e) Propeller speed reference. (f) Flap angle reference.

increased to assume the wind disturbance situation as shown in Fig. 10(a). Figs. 10(b) and 10(c) show that the tracking performance with the conventional method deteriorates due to the wind disturbance because the flap actuator saturates as shown in Fig. 10(f). On the contrary, the proposed method can maintain the command velocity by changing the tilt angle even when the wind disturbance is applied. The result, which is almost the same as Fig. 7, shows that the proposed method has better performance when the wind disturbance exists.

## V. CONCLUSION

In this paper, we proposed a wing angle correction method which produces the wing angle reference considering the achievable acceleration field. In the simulation, the proposed method has better tracking performance than the conventional method even where the high-acceleration situation or the wind disturbance situation, and the HILS result of the wind disturbance situation shows almost the same result as the

simulation result. In the future, we will validate the proposed method through flight tests.

## ACKNOWLEDGMENT

This work was partly supported by JSPS KAKENHI Grant Number JP23H00175.

## REFERENCES

- [1] L. A. Garrow, B. J. German, and C. E. Leonard, "Urban air mobility: A comprehensive review and comparative analysis with autonomous and electric ground transportation for informing future research," *Transportation Research Part C: Emerging Technologies*, vol. 132, p. 103377, 2021.
- [2] B. Mishra, D. Garg, P. Narang, and V. Mishra, "Drone-surveillance for search and rescue in natural disaster," *Computer Communications*, vol. 156, pp. 1–10, 2020.
- [3] M. T. Fard, J. He, H. Huang, and Y. Cao, "Aircraft distributed electric propulsion technologies—a review," *IEEE Transactions on Transportation Electrification*, vol. 8, no. 4, pp. 4067–4090, 2022.
- [4] C. Yu, Y. Zheng, B. Shyrokau, and V. Ivanov, "MPC-based path following design for automated vehicles with rear wheel steering," in *2021 IEEE International Conference on Mechatronics (ICM)*, pp. 1–6, 2021.
- [5] J. C. Escobar, A. Castillo, P. Castillo, and P. García, "Reactive and predictive control scheme for evasive maneuvers in aerial robots," *IEEE Transactions on Aerospace and Electronic Systems*, vol. 59, no. 6, pp. 8614–8623, 2023.
- [6] Y. Tsuji, D. Yashiro, Y. Kato, S. Bando, K. Yubai, and S. Komada, "Design of a thrust controller for propeller driven systems operating at multiple wind velocities and propeller angular velocities," *IEEJ Journal of Industry Applications*, vol. 12, no. 6, pp. 1060–1067, 2023.
- [7] K. Yokota and H. Fujimoto, "Pitch angle control by regenerative air brake for electric aircraft," *IEEJ Journal of Industry Applications*, vol. 11, no. 2, pp. 308–316, 2022.
- [8] K. Yokota and H. Fujimoto, "Aerodynamic force control for tilt-wing eVTOL using airflow vector estimation," *IEEE Transactions on Transportation Electrification*, vol. 8, no. 4, pp. 4163–4172, 2022.
- [9] Y. Naoki, S. Nagai, and H. Fujimoto, "Mode-switching algorithm to improve variable-pitch-propeller thrust generation for drones under motor current limitation," *IEEE/ASME Transactions on Mechatronics*, vol. 28, no. 4, pp. 2003–2011, 2023.
- [10] M. Sato and K. Muraoka, "Flight controller design and demonstration of quad-tilt-wing unmanned aerial vehicle," *Journal of Guidance, Control, and Dynamics*, vol. 38, no. 6, pp. 1071–1082, 2015.
- [11] P. Hartmann, C. Meyer, and D. Moormann, "Unified velocity control and flight state transition of unmanned tilt-wing aircraft," *Journal of Guidance, Control, and Dynamics*, vol. 40, no. 6, pp. 1348–1359, 2017.
- [12] D. Rohr, T. Stastny, S. Verling, and R. Siegwart, "Attitude and cruise control of a VTOL tiltwing UAV," *IEEE Robotics and Automation Letters*, vol. 4, no. 3, pp. 2683–2690, 2019.
- [13] D. Rohr, M. Studiger, T. Stastny, N. R. J. Lawrance, and R. Siegwart, "Nonlinear model predictive velocity control of a VTOL tiltwing UAV," *IEEE Robotics and Automation Letters*, vol. 6, no. 3, pp. 5776–5783, 2021.
- [14] T. Katagiri, K. Yokota, K. Fujimoto, S. Nagai, and H. Fujimoto, "Basic study on velocity control in wing coordinate system using acceleration-based disturbance observer for tilt-wing eVTOL," in *The 10th IEEJ International Workshop on Sensing, Actuation, Motion Control, and Optimization (SAMCON2024)*, pp. 115–120, IEEJ, 2024.
- [15] B.-M. Nguyen, T. Kobayashi, K. Sekitani, M. Kawanishi, and T. Narikiyo, "Altitude control of quadcopters with absolute stability analysis," *IEEJ Journal of Industry Applications*, vol. 11, no. 4, pp. 562–572, 2022.
- [16] E. Sariyildiz, H. Sekiguchi, T. Nozaki, B. Ugurlu, and K. Ohnishi, "A stability analysis for the acceleration-based robust position control of robot manipulators via disturbance observer," *IEEE/ASME Transactions on Mechatronics*, vol. 23, no. 5, pp. 2369–2378, 2018.